
Chapter 3

Shatter cones

3.1 Introduction

Shatter cones are a distinct, mesoscopic and impact-diagnostic feature. These typically striated cone-shaped fractures (Fig. 3.1) have been known for a long time from many impact sites around the world, e.g., from the Steinheim Basin in Germany, where they were referred to as “Strahlenkegel” (Branco and Fraas 1905), from the USA (e.g., Kentland structure, Shrock and Malott 1933; Wells Creek, Bucher 1936; Sierra Madera, Dietz 1960), Canada (e.g., Sudbury, Dietz 1964; Clearwater Lake, Dence 1964; Manicouagan, Dietz 1968), Africa (Vredefort, Dietz 1961, Hargraves 1961) and Australia (Gosses Bluff, Cook 1966, Crook and Cook 1966), well before impact was recognised as the likely cause of most of these structures.

Shatter cones represent a rock fracture phenomenon with more or less curved fracture surfaces that are characterized by generally divergent striations. They are distinctive in appearance and show some important differences to slickensides (see, e.g., French 1998, and references therein; Lugli et al. 2005). The striae typically emanate from the apex of a conical fracture and diverge distinctly, so that the base of a shatter cone segment is usually wider than the apex area (Fig. 3.1). Striations are not necessarily straight and, in places, may be distinctly curved, especially further from the apex (Fig. 3.2). In cases where striations are subparallel to parallel (see section 3.4.3), they can still be distinguished from those on slickensides, which are characterized by a diagnostic unidirectional step-like pattern that actually allows investigation of the sense of movement on such fractures (e.g., Passchier and Trouw 1996), and by having sharp, angular shapes of the ridges. In contrast, striations on shatter cone surfaces are distinctly rounded (Nicolaysen and Reimold, 1999). Lugli et al. (2005) provided extensive discussion of the recognition criteria of shatter cones and the difficulties to distinguish this impact deformation phenomenon from cone-in-cone structures and the products of other geological processes (tectonics, wind ablation, sedimentary percussion marks).



Fig. 3.1: Typically conical appearance of a shatter cone from the Houghton Structure in Canada. Sample courtesy of B.O. Dressler.

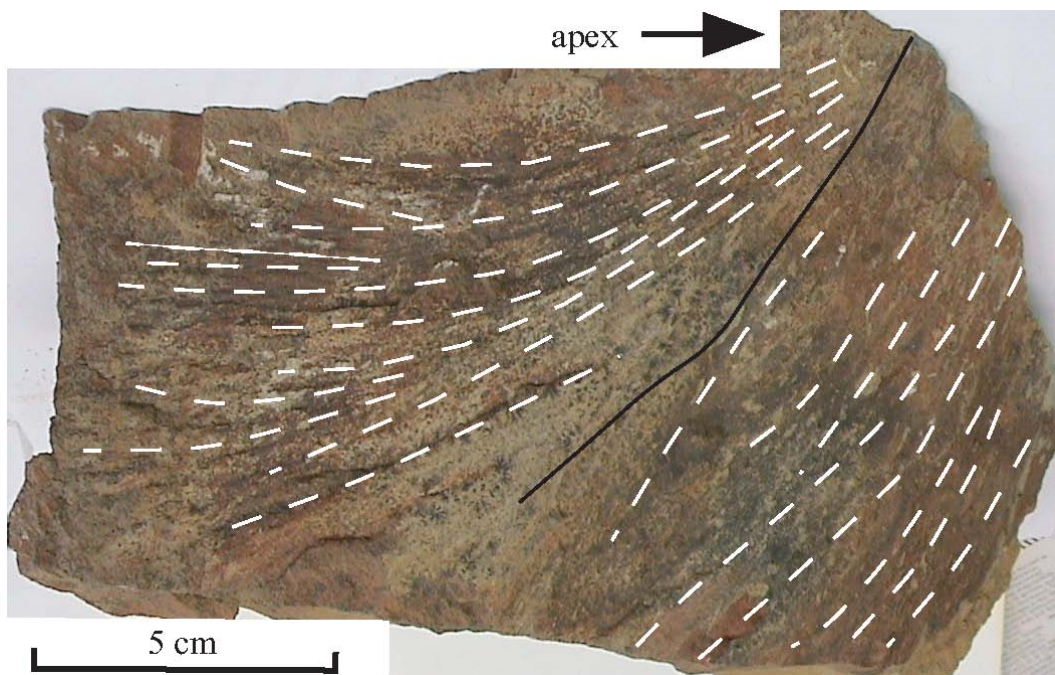


Fig. 3.2: A shatter cone sample from the Booyens Shale location in the northwestern part of the collar of the Vredefort Dome (location 2, see Appendix No. 6). The striations branch radially off the apex (to the top right), which is the typical appearance of striations. However, at the end of the segment (bottom left), the striations (dashed lines) are strongly curved and terminate into a subhorizontal fracture. The intersection between two fractures belonging to a set of two sets of MSJS is shown with a black line.

Dietz (1947, 1959, 1964) must be credited with establishing shatter cones as a diagnostic shock deformation feature of meteorite impact structures, with his thorough analytical work especially in the Kentland and Sudbury structures. Since then, shatter cones have been observed in a large number of confirmed impact structures (e.g., French 1998), and their presence is regarded as a telltale recognition criterion for such structures. Whilst a significant body of field, laboratory and

numerical modeling work on shatter cones has been established, some of it in recent years (e.g., Milton 1977; review by French 1998; Gibson and Spray 1998; Nicolayson and Reimold 1999; Sagy et al. 2002, 2004; Baratoux and Melosh 2003), the process by which shatter cones are developed is still under debate.

This study provides new field observations on shatter cone structures, including their forms, their striation geometry, and their relationship to other structural features, in the northern and western collar of the Vredefort Dome. These data and observations are used to evaluate two recent hypotheses for shatter cone formation (Sagy et al. 2002, 2004; Baratoux and Melosh 2003).

3.2 Background

3.2.1 General observations on shatter cones

Shatter cones can be found in almost all rock types affected by shock deformation, i.e., sedimentary as well as crystalline rocks (e.g., at Clearwater Lake, Dence 1964). The early work also showed that, usually, fine-grained and more homogeneous rock types were favored for shatter cone formation (e.g., Dietz 1961; also: Gosses Bluff, Cook 1966, Milton et al. 1996; Vredefort, Manton 1965, this study). Furthermore, the number of inclusions in a rock, i.e., the grade of inhomogeneity, appeared to play a role in determining the relative intensity of shatter coning. In other words, the more homogeneous a rock, the less shatter coning can be expected in this rock type. The size of a cone cannot be predicted with any certainty from rock properties. Cones between several metres (e.g., Dressler et al. 1999) and millimetres in size have been observed.

Shock experiments (Milton 1977; Roddy and Davis 1977; Sharpton et al. 1996) revealed that shatter cones can be formed at minimum shock pressures of 4 ± 2 GPa, which would place them into the periphery or “ring zone” around central uplifts (e.g., Sudbury, Dietz 1964). However, this fracture phenomenon has also been observed within the central uplifts of impact structures, where shock pressures may have been as high as 30 GPa, such as the Steinheim Basin (Branco and Fraas 1905), Kentland (Shrock and Malott 1933; Dietz 1947), Manicouagan (Dietz 1968), and Sierra Madera (Wilshire et al. 1972). At some impact sites, shatter cones were found in the innermost parts of the rim zone of central uplifts, e.g., at Sierra Madera (Dietz 1960; Wilshire et al. 1972), Gosses Bluff (Cook 1966; Crook and Cook 1966; Milton

et al. 1996) and at Vredefort (Hargraves 1961; Minnitt et al. 1994; this study). Osinski and Spray (2005) observed shatter cones in the central parts of the 23 km diameter Haughton impact structure, as well as in crater-fill impact melt rocks and megablocks of the ejecta blanket. They interpreted these findings as indicative of shatter cone formation in a very early stage of cratering (contact and compression stage).

Dietz's (1959, 1961) concept of systematic geometric orientation of shatter cones received support from many authors (e.g., Hargraves 1961; Manton 1965; French 1998). This hypothesis proposes that shatter cone apices observed in sedimentary strata display a preferred orientation with regard to the bedding orientation of the host rock: in originally horizontal target strata, most shatter cone apices would be oriented at a high angle to bedding and, hence, point upwards. Wilshire et al. (1972), however, found that cone segments in the Sierra Madera impact structure were randomly oriented relative to bedding and that they were preferentially developed on joint and bedding surfaces. They concluded that the distribution of shatter cones was irregular due to the dependence of cone orientation on lithological and structural variation.

3.2.2 Previous observations on shatter cones in the Vredefort Dome

The existence of full cones in the Vredefort Dome has been reported by, *inter alia*, Mayer and Albat (1990), Mayer (1997) and French (1998). This is in contrast to most other observations at Vredefort (e.g., Manton 1965; Nicolaysen and Reimold 1999; this study) that showed that, in general, what has been described as shatter cones are typically only partial cone fractures (examples shown in Figs. 3.2, 3.14). Where full 360 degree cone fractures have been described, both the apices and the lower cone circumferences can be broken up into distinct segments representing individual fractures of curvilinear geometry (see, e.g., figures in Mayer 1997), consistent with the multipli-striated joint (MSJ)/shatter cone link promoted by Nicolaysen and Reimold (1999).

Albat (1988) reported that shatter cone orientations in the Vredefort Dome were constant with respect to the bedding orientation and concluded that shatter cones formed prior to the overturning of the strata, in agreement with Hargraves (1961) and Manton (1962) but in contrast to Simpson's (1981) findings in the dome. Simpson (1981) observed shatter cones on fault gouge presumed to be the result of Vredefort

impact deformation, which challenged the view of an origin during shock compression. Reimold and Colliston (1994) reported on a location on farm Gatoma in the western collar of the Vredefort Dome, where shatter cones were observed superimposed on pseudotachylitic breccia. These authors consequently raised the question whether the formation of shatter cones takes place early in the cratering process. However, the possibility of a pre-impact timing for the formation of such pseudotachylitic breccias could not be ruled out by these authors (compare also Berlenbach and Roering 1992; Reimold et al. 2005). It is of interest that since that work no such case of superposition of shatter coning onto pseudotachylitic breccia in the Vredefort Dome has been observed.

Nicolaysen and Reimold (1999) inferred from detailed outcrop studies in the dome that an inherent relationship exists between shatter cones and intersecting, closely-spaced sets of MSJ, a type of fracture that is characterised by a distinctly curvilinear geometry at both the microscopic and megascopic scale. In Figs. 3.3a and b three distinct, closely-spaced sets of such fractures of subplanar, slightly undulating geometry are emphasized. In support of this relationship between striated surfaces and fractures, these authors noted that the striations on these surfaces typically plot in stereographic projections around the intersections between MSJS of different orientations. MSJS were introduced as a distinct type of fractures, which could be studied at all scales between metre-spaced and sub-microscopic fractures and were also reported from the Sudbury Structure by these authors.

Albat and Mayer (1989) described so-called shock-fractures (“S-fractures”) from the collar of the Vredefort Dome that displayed a conjugate pattern and which they related to shatter cone formation. Nicolaysen and Reimold (1999; also Nicolaysen and Reimold, 1987, wherein the concept of multipli-striated joint surfaces was first introduced) concluded that Albat and Mayer (1989) had selected only one pair of MSJ sets, while neglecting the other MSJ orientations present at all outcrops throughout the collar of the Vredefort Dome. They observed sets of MSJ in up to 12 orientations at specific outcrops. Martini (1991) could not find any correlation between his so-called “A-type (early-formed, under shock compression) pseudotachylite” veins (see Chapter 5) and “S-surfaces”, which he also related to the formation of shatter cones. He did report thin coats of melts on shatter cone surfaces, but did not relate them to the melt vein phenomenon. Melt formation on shatter cone

Fig. 3.3: (a) Several closely-spaced sets of fractures of different orientations (indicated by numbers) on a quartzite boulder from the Schurwedraai alkali-granite complex in the northern part of the collar. At the end of the planar surface on top of the boulder, striated surfaces are obvious, which correspond to the differently oriented traces on the main surface; the frame indicates area shown in Fig. 3.3b. (b) Close-up of the striated surfaces of the inset area in a), illustrating the relationship of striated surfaces to closely-spaced sets of fractures (MSJS, concept of Nicolaysen and Reimold, 1999). Corresponding striated surfaces and related fractures are indicated in (a) and (b) with the same numbers. Pen for scale in a) and b) ca. 10 cm. Both photographs courtesy of W.U. Reimold.

surfaces has also been described by Gay (1976), Gay et al. (1978), Simpson (1981), and Gibson and Spray (1998), as well as by Nicolaysen and Reimold (1999), who noted the presence of microscopic melt pockets at intersections of MSJ microfractures.

Some authors (e.g., Hargraves 1961; Manton 1965; Milton 1977; Albat 1988; Albat and Mayer 1989) claimed that, where small shatter cones vary in orientation over a small area, they belong - and can be geometrically confined - to a larger “master cone”. This means that all orientations of shatter cone striations within a limited geographic area would fall on a small circle when plotted onto a stereonet, and that the axis of this circle forms the single invariant feature of the shatter cone exposure. Striations on cone surfaces from the Vredefort impact structure were plotted in this way and “master cone” axes were inferred. After back-rotation of the host stratum into its perceived horizontal pre-impact orientation, these so-called “master cone” apices pointed towards and above the centre of the dome, i.e. towards the original locus of the projectile explosion. Nicolaysen and Reimold (1999), however, disputed this method on the grounds of sampling bias, suggesting that only selected measurements had been obtained and that all possible orientations of shatter cones had not been included in construction of “master cone” data sets. Their own statistical approach failed to produce any small-circle patterns.

3.2.3 Hypotheses on shatter cone formation

3.2.3.1 *Overview of past hypotheses*

Although Dietz (1959, 1961, 1968) interpreted shatter cones as the product of fracturing caused by the passage of an impact-generated shock wave, he did not provide other specific details on their mechanism of formation. Johnson and Talbot (1964) suggested that shatter cones form when the elastic precursor wave of an impact-produced shock wave is refracted by an inhomogeneity in the target rock, such as changes in lithology, structural heterogeneities and varied grain size of minerals. Gash (1971) proposed a similar model, involving interference of the shock wave with a tensile wave that is reflected by heterogeneities in the target rock (see also, Hargraves 1961; Manton 1962, 1965; Albat 1988; Albat and Mayer 1989).

3.2.3.2 Recent hypotheses: Baratoux and Melosh (2003)

These workers applied numerical modelling to investigate the possibility of scattering, refraction, and/or reflection of a shock wave during its propagation through the target rocks. Their results suggest that the size and distribution of shatter cones could be linked to the shock front width (or rise time of the shock wave) and the size of heterogeneities in the affected lithologies, and that reflection of a shock wave is caused by heterogeneities within a lithological unit. Baratoux and Melosh (2003) proposed that shatter cones are tensional fractures, formed at a local heterogeneity, which could be a pre-existing fracture, porosity or mineral/matrix components with different elastic properties. They concluded that, when the shock wave meets a heterogeneity, an extensional wave is generated, propagating radially outward from the heterogeneity (Fig. 3.4). In this hypothesis, scattered elastic waves interfere with the main stress wave in spherical geometry, leading to an increase in tensional stress and, therefore, curved fractures (Fig. 3.5). Depending on the shape of this heterogeneity, the interaction of the waves creates a conical (e.g., grains or voids), planar, paraboloid or hyperboloid fracture surface.

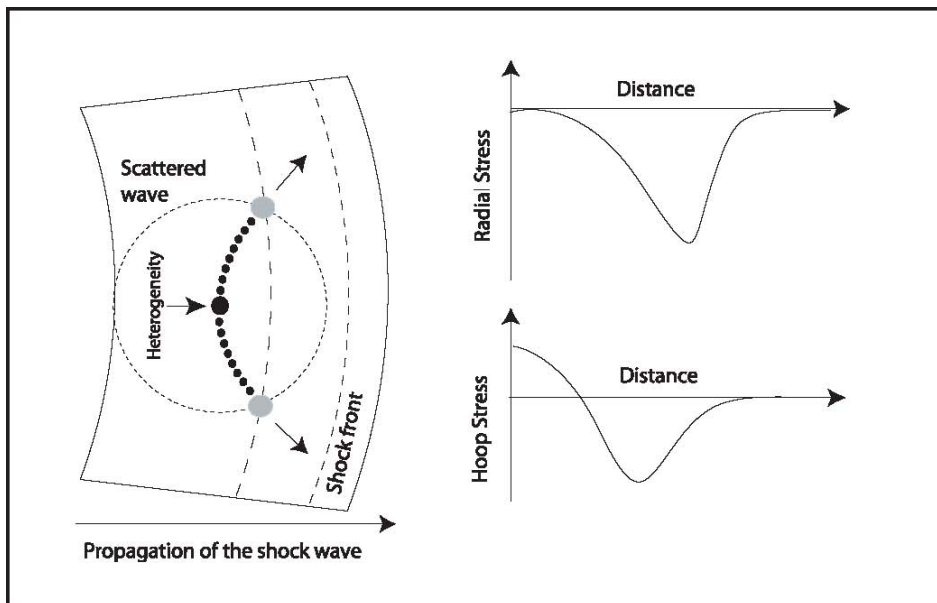


Fig. 3.4: Schematic representation for the formation of shatter cones after Baratoux and Melosh (2003). Tensile fracture occurs at the intersection between the scattered tensile wave and the tensile hoop stresses in the main shock wave. When a critical value for the tensional stress is reached, the rock fracture is in tension. The fractures accumulate on the surface of a conical region (indicated by filled circles and arrows; taken from Baratoux and Melosh 2003). The right diagram illustrates the intensity of the radial and the hoop stress with distance.

Baratoux and Melosh (2003) concluded that shatter cone formation might only take place in the post-shock phase of the compression stage of cratering, when the rarefaction wave propagates through the target rocks and interferes with scattered waves generated when the shock front encounters the heterogeneities in the strata.

3.2.3.3 *Sagy et al. (2002, 2004)*

These authors observed in the Kentland Structure and in the Vredefort Dome that shatter cone surfaces are curved, oblate, and spoon-like rather than truly conical. Furthermore, they related this to the fact that shatter cone fracturing is penetrative and pervasive within the rock body and concluded that the shatter cone geometry is an “intrinsic 3-D structure [produced by] multilevel branching” (Sagy et al. 2002, 2004). They also proposed that shatter cones are tensile fractures. Sagy et al. (2002, 2004) supported this with observations of diverging pairs of striations on shatter cone surfaces and the absence of measurable shear displacement along their surfaces (Fig. 3.6). This figure illustrates the characteristics of tensile fracture front waves when hitting a heterogeneity in the target rock and creating an angle α that is responsible for the typical “V”-pattern of shatter cone striations. This is in sharp contrast to observations of micro-displacements by Nicolaysen and Reimold (1999). In addition, Sagy et al. interpreted thin coats of melt on shatter cone surfaces as the result of rapid tensile fracturing by decompression in brittle materials rather than sliding (friction) induced melting.

These authors found that striations on shatter cone surfaces typically occur as pairs, creating a V-like structure on the surface and defining the so-called “V-angle” α (Figs. 3.6 and 3.7). According to Sagy et al. (2004), these “V-striations” are formed by a front wave (FW), which is present at the leading edge of a rapidly moving fracture front and that is excited when this fracture front comes into contact with a heterogeneity in the target rock (Fig. 3.6). The front wave that emanates from this heterogeneity produces tracks on the fracture surface that are represented by the “V-striations”. Sagy et al. (2004) concluded that the speed of the fracture front waves is rather constant over the range of a single shatter cone sample and, thus, the “V-angles” (striation angles) must also be consistent. They substantiated this hypothesis with observations from Kentland and Vredefort, where they found these “V-angles” to be relatively constant on a single shatter cone surface, with a typical standard

Fig. 3.5: (a) Stress history of a shock wave at a heterogeneity showing the time (x-axis) at which the tensional stress exceeds the (average) minimum stress required for damage accumulation. This plot illustrates how the stress responsible for the fragmentation propagates along the boundary of a cone as discussed in the text. (b) Time at which complete damage occurs. Damage accumulates when the tensional stress is greater than the minimum stress. The two plots are not exactly identical, as the maximum stress, which depends on the size of the cells (y-axis) that can be modelled, varies along the radius of the spherical shell (taken from Baratoux and Melosh 2003).

Fig. 3.6: Characteristics of fracture front waves (FW) on the surfaces of rapid tensile fractures. The FW form when the front of a rapid fracture encounters an obstacle in the target rock. The distinct V-shaped tracks of FW are shown in the fracture surface photographs of (a) glass and (b) artificial rock. All fractures in the figures propagated from left to right in all images. The FW tracks, marked by the two diverging arrows, emanate from their source at an angle α . (c) Comparison between the V striations (top of figure c) in different rock types and the experimentally observed FW tracks (bottom of figure c): FW marks in glass (left) and V striations on quartzite (middle) and slate (right) shatter cones (top of figure c); diagrams of FW tracks associated with these samples (bottom of figure c); each line in the diagram denotes a pair of propagating pulses, propagating along the moving fracture front, at specific times (taken from Sagy et al. 2004).

deviation, for a given shatter cone sample, of 4° to 9° , but that values could vary from sample to sample in the same location. They conducted a statistical evaluation of measurements of “V-angles” from samples of different rock types and found that the

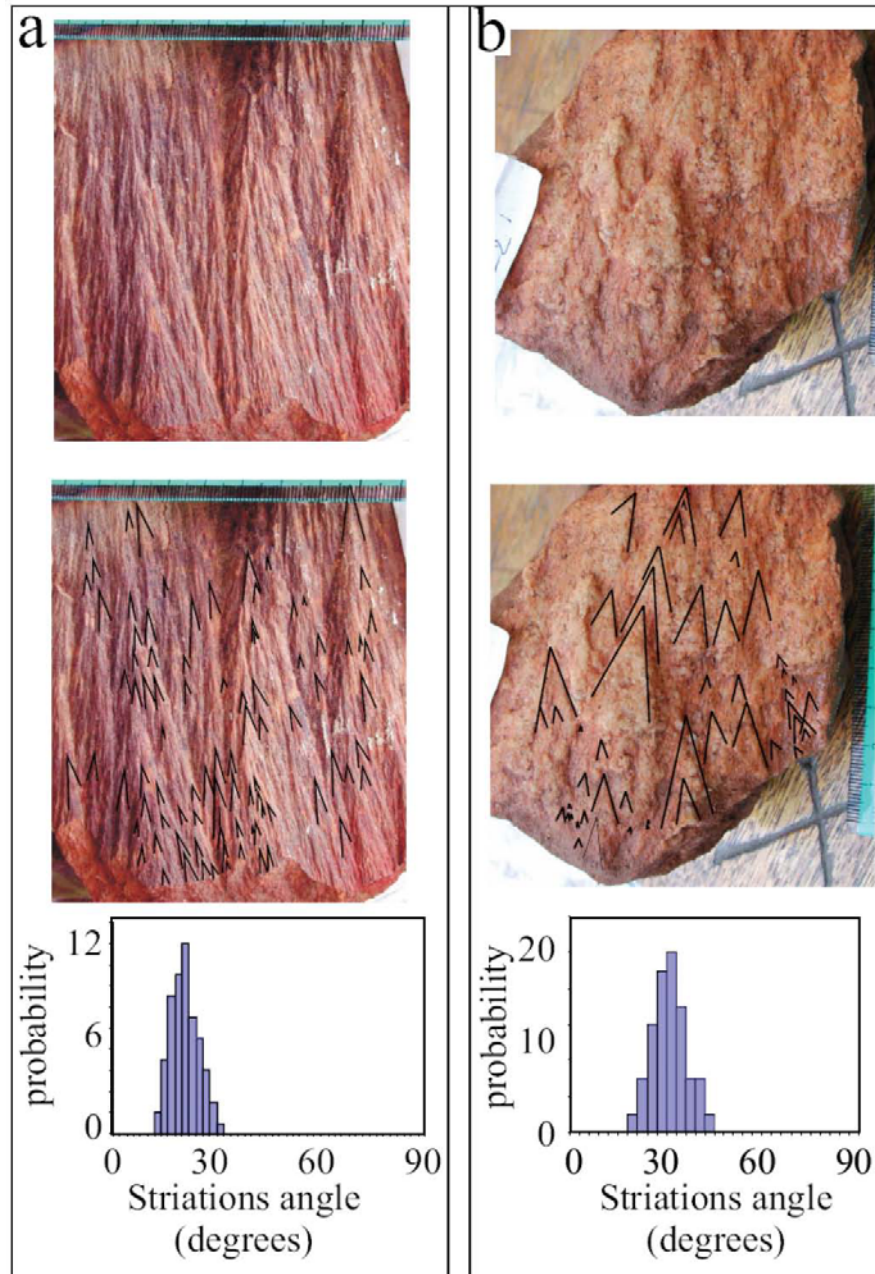


Fig. 3.7: Display of the striations on the surfaces of shatter cones in (a) slate and (b) quartzite from the Vredefort Dome (taken from Sagy et al. 2004). The striations are arranged in V-shaped pairs, termed V striations, and enclose a vertex angle termed V angle. The images at top show the respective two shatter cone surfaces, and in the centre images the marked V angles are presented. The histograms in the bottom row show the frequency distributions of the V angles, with mean values of $21^\circ \pm 4$ (85 measured) and $31^\circ \pm 6$ (43 measured) for the slate and quartzite samples, respectively. From the determination of the mean angles, these authors attempted to determine the fracture propagation velocities for several types of deforming rock (Fig. 3.8).

mean angles are consistent for samples from a similar distance from the centre of the Vredefort Dome, but that the mean angles increased from 17° to 46° with increasing radial distance (15 km to 40 km). The increase of the mean angle with radial distance from the centre of the impact structure was attributed to the decreasing speed of the fracture front farther from the centre of the impact structure (Fig. 3.8). Although these mean angles were fairly constant on individual samples, these authors did report range of individual V-angles from $\sim 10^\circ$ to 30° for specific sites (compare Fig. 3.7), and, thus, did not consider the actual variation of striation angles at specific sample sites.

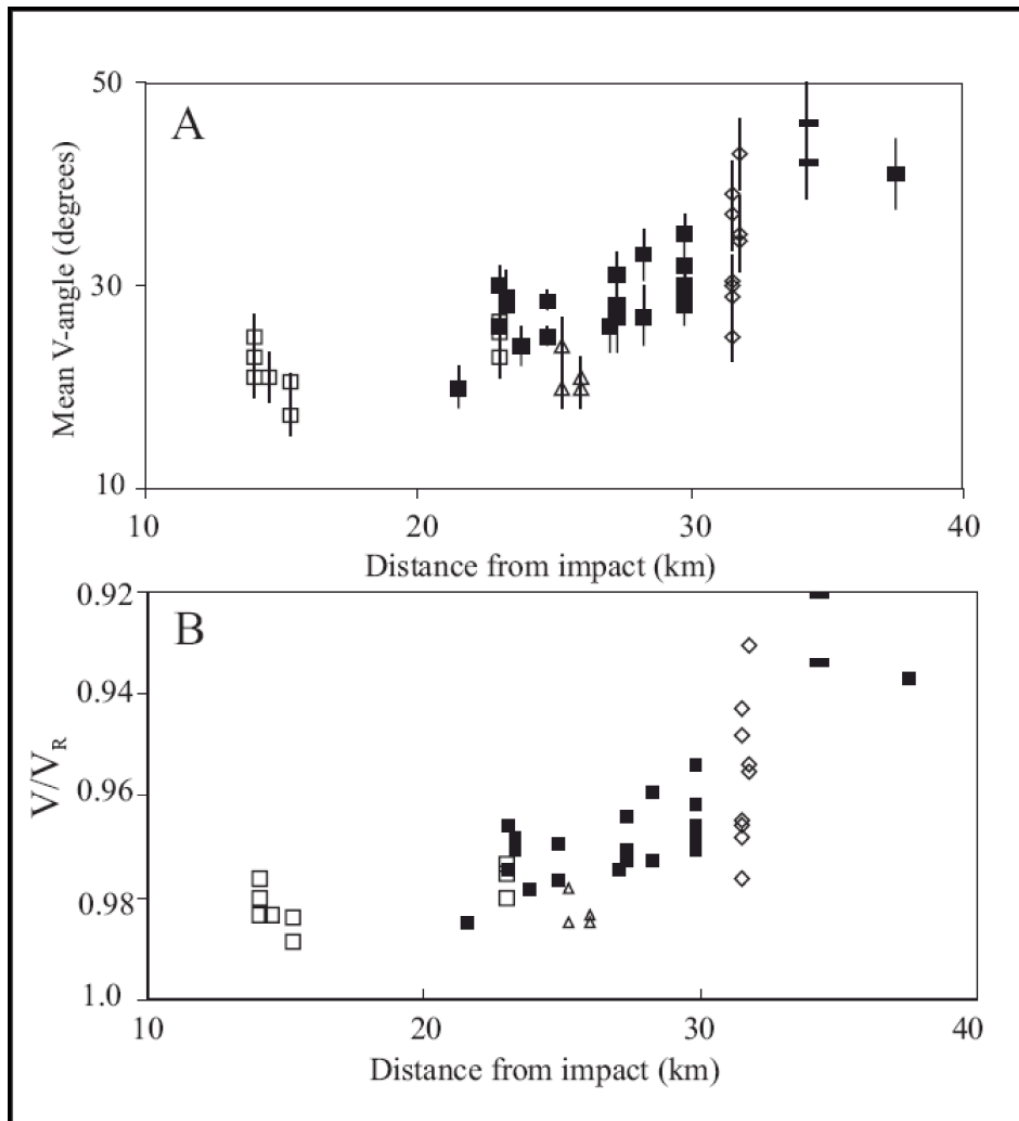


Fig. 3.8: V angles of shatter cone striations measured at sites from the Vredefort Dome, and the associated propagation velocity, V/V_R (r = radius from the centre of the dome). (a) Systematic increase of α (mean angle between a pair of striations) with distance from the impact centre as measured for samples collected at numerous sites, which include granite (open squares), quartzite (solid squares), slates (triangles), andesite (diamonds), and chert (bars). (b) Normalized fracture velocity, V/V_R , versus distance from the impact centre in Vredefort (taken from Sagy et al. 2004).

3.3 Methodology for this study

In the course of this study, 43 locations with striated surfaces, that is, either well developed shatter cones or fracture surfaces of more planar geometry (see section 3.4.2) thought to be related to shatter cones, were documented in detail (see Table 3.1). A further 30 locations contained other striations (e.g., lineations, slickenside striae) that could not be unequivocally related to shatter cones (for locations see Appendix No. 6). These locations are, therefore, not included in Fig. 3.9 and Table 3.1. Most of the 43 shatter cone locations contained either incomplete segments or only one or two striated surfaces that were not statistically meaningful. The rest of these locations, that are highlighted in Fig. 3.9 and Table 3.1, contained sufficient striated surfaces of acceptable quality and were used for the statistical treatment of observations in this investigation. *In situ* striation orientation measurements were made on shatter cones at these sites throughout the collar. In addition, oriented shatter cone samples were collected from a number of sites in the northern and northwestern parts of the collar, up to 65 km from the centre of the dome (Fig. 3.9). GPS coordinates for selected locations that are discussed in detail are given in Table 3.1. Studied sites occur in different lithological units of the Witwatersrand, Ventersdorp and Transvaal supergroups. The strata investigated were predominantly quartzites, but also include some shales (Booyens shale and Coronation shale, part of the Witwatersrand Supergroup, see Fig. 1.9) and meta-volcanic rocks (Ventersdorp Supergroup and Hekpoort Formation of the Transvaal Supergroup, see Fig. 1.9). Furthermore, samples from other impact sites (Steinheim, Houghton) were kindly made available by a number of colleagues and were used for comparison with the Vredefort shatter cones.

Striation measurements on shatter cone surfaces (both *in situ* and on oriented laboratory samples) were made on as many available surfaces as possible. Measurements for three specific and representative (in terms of the entire database) sites are shown on stereonet. From these plots, the form of each shatter cone surface and (where *in situ*) the orientation of the cone apex were determined. Also, following the concept of Sagy et al. (2002, 2004), so-called “mean striation angles” were determined on striated surfaces at three sites (locations 2, 594 and 680) from the inner and outer parts of the collar, as well as from the core of the dome (location 2, location 279 and location 594, respectively; see Table 3.1 and Fig. 3.9). Samples from a traverse between sites 38 and 514 (compare Fig. 3.9) were used to determine striation

Table 3.1: List of shatter cone locations in the collar rocks of the Vredefort Dome. Locations that are referred to in detail in the text are highlighted.

location	~Distance from centre	GPS coordinates	Average bedding orientation (dip dir./dip)	Lithology
1	30	S 26° 51' 12. 0" E 027° 17' 04. 0"	145/ 70	Johannesburg Quartzite
2	30	S 26° 45' 24. 1" E 027° 30' 12. 1"	199/ 77	Turffontein Quartzite
38	20	S 26° 49' 36. 9" E 027° 29' 35. 3"	177/ 64	Hospital Hill Quartzite
59	20	S 26° 49' 51. 7" E 027° 28' 37. 0"	305/ 56	Hospital Hill Shale
69	22	S 26° 49' 37. 3" E 027° 28' 12. 2"	346/ 54	Hospital Hill Quartzite
72	22	S 26° 49' 34. 9" E 027° 28' 20. 6"	347/ 60	Government Quartzite
73	22	S 26° 49' 33. 2" E 027° 28' 26. 9"	345/ 54	Government Quartzite
82	22	S 26° 49' 25. 3" E 027° 29' 02. 6"	163/ 59	Government Quartzite
99	27	S 26° 48' 00. 3" E 027° 28' 47. 4"	038/ 56	Johannesburg Quartzite
100	27	S 26° 47' 55. 0" E 027° 28' 34. 8"	027/ 59	Johannesburg Quartzite
101	27	S 26° 47' 48. 0" E 027° 28' 24. 7"	037/ 46	Johannesburg Quartzite
107	27	S 26° 47' 48. 4" E 027° 29' 52. 0"	212/ 64	Johannesburg Quartzite
109	27	S 26° 47' 59. 3" E 027° 30' 07. 9"	207/ 17	Johannesburg Quartzite
125	30	S 26° 47' 15. 6" E 027° 29' 26. 4"	164/ 73	Johannesburg Quartzite
136	35	S 26° 45' 41. 0" E 027° 29' 34. 3"	135/ 40	Turffontein Quartzite
180	20	S 26° 51' 19. 2" E 027° 25' 21. 5"	139/ 51	Hospital Hill Quartzite
231	20	S 26° 51' 04. 9" E 027° 23' 39. 7"	147/ 53	Government Quartzite
237	20	S 26° 51' 15. 5" E 027° 23' 05. 6"	171/ 56	Government Quartzite
279	26	S 26° 51' 43. 3" E 027° 15' 56. 8"	180/ 54	Johannesburg Quartzite
306	35	S 26° 48' 43. 9" E 027° 23' 05. 9"	176/ 70	Turffontein Quartzite
328	35	S 26° 47' 58. 3" E 027° 22' 51. 8"	169/ 27	Turffontein Quartzite
360	32	S 26° 48' 07. 2" E 027° 24' 21. 6"	127/ 58	Turffontein Quartzite
361	32	S 26° 48' 08. 9" E 027° 24' 18. 1"	143/ 43	Turffontein Quartzite
362	32	S 26° 48' 08. 7" E 027° 24' 15. 2"	143/ 54	Turffontein Quartzite

366	30	S 26° 49' 17. 6" E 027° 24' 33. 3"	151/ 52	Turffontein Quartzite
402	25	S 26° 51' 05. 3" E 027° 20' 24. 6"	--	Alkali Granite
404	25	S 26° 51' 08. 8" E 027° 20' 25. 0"	166/ 48	Government Quartzite
481	35	S 26° 52' 22. 2" E 027° 15' 02. 5"	153/ 53	Turffontein Quartzite
483	35	S 26° 52' 10. 6" E 027° 15' 22. 7"	144/ 61	Turffontein Quartzite
484	35	S 26° 52' 06. 8" E 027° 15' 23. 0"	144/ 66	Turffontein Quartzite
485	35	S 26° 52' 02. 0" E 027° 15' 23. 3"	139/ 58	Turffontein Quartzite
497	35	S 26° 51' 44. 4" E 027° 15' 43. 5"	158/ 64	Turffontein Quartzite
500	35	S 26° 51' 43. 3" E 027° 15' 56. 8"	153/ 46	Turffontein Quartzite
514	65	S 26° 26' 08. 2" E 027° 30' 02. 1"	--	Timeball Hill Quartzite
518	40	S 26° 44' 38. 7" E 027° 30' 01. 1"	--	Ventersdorp Lavas
519	35	S 26° 45' 24. 1" E 027° 30' 12. 1"	199/77	Turffontein Quartzite
571	22	S 26° 54' 49. 5" E 027° 17' 47. 6"	147/ 55	Hospital Hill Quartzite
594	10	S 27° 08' 35. 4" E 027° 37' 30. 2"	--	Greenstone Complex
606	20	S 26° 50' 19. 4" E 027° 33' 31. 5"	343/ 60	Hospital Hill Quartzite
637	35	S 26° 54' 27. 1" E 027° 12' 09. 7"	126/ 44	Turffontein Quartzite
638	35	S 26° 56' 00. 2" E 027° 11' 33. 6"	103/ 59	Turffontein Quartzite
639	35	S 26° 56' 01. 1" E 027° 11' 52. 2"	152/ 36	Turffontein Quartzite
680	30	S 26° 58' 13. 7" E 027° 12' 34. 6"	072/ 51	Turffontein Quartzite
819	15	S 26° 53' 35. 9" E 027° 24' 43. 7"	--	Archean basement

angles in order to test the proposal by Sagy et al. (2002, 2004) that striation angles decreased in a systematic fashion with increasing distance from the centre of an impact structure.

3.4 Results

3.4.1 Distribution and occurrence of shatter cones in the collar of the Vredefort Dome and environs

Taking into consideration that the quartzite units are generally better exposed than the less competent shale units in the collar of the Vredefort Dome, most shatter cone-related striations were naturally found in the quartzite units of the Witwatersrand Supergroup. However, road-cuts in the northwestern part of the collar (e.g., location 2, Fig. 3.9 and Table 3.1) expose shales with abundant, well-developed shatter cones (Fig. 3.10a and b). The greater abundance of striated surfaces at location 2 (see Fig. 3.9 and Table 3.1), compared with far fewer shatter cone surfaces in the directly adjacent quartzites, confirms a preferred development of shatter cones in fine-grained lithologies, as first suggested by Dietz (1961) and since supported by other workers (see, e.g., Manton 1962, 1965; Nicolaysen and Reimold 1999). While the limited exposure of the shales did not allow us to comprehensively test the variation in intensity of shatter cone development along radial traverses outwards from the interior of the dome, it was found that shale horizons with intense development of shatter cones do occur over a narrow, arcuate sector of the supracrustal collar, spanning a radial distance of no more than 20 km between the inner collar (~20 km from the centre of the dome) and the outer collar (~40 km from the centre). This suggests that main shatter cone development occurs in a rather narrow shock pressure regime, namely just below the regime characterized by single sets of planar deformation features (PDF) in quartz corresponding to shock pressures between ca. 8 and 15 GPa (Stöffler and Langenhorst 1994; Huffman and Reimold 1996; also compare the regional shock deformation study of Gibson and Reimold 2005). Thus, maximum shatter cone development in shales is observed in the zone of < 8 GPa shock pressure, consistent with earlier estimates (e.g., French 1998, and references therein).

However, reports from higher-pressure zones in other impact structures (e.g., in the range from >10-45 GPa, at Sudbury – e.g., French 1998 and references therein), evidence that shock pressures are actually highly heterogeneous on a variety of scales in the Vredefort Dome (Gibson and Reimold 2005), and that rocks in the dome experienced increasing degrees of recrystallization and annealing towards the

Fig. 3.9: Schematic geological map of the Vredefort Dome, showing the stratigraphy and the main impact-related features. The shatter cone limit by Therriault et al. (1997) is also given. Filled black circles indicate sites from where samples of shatter cone segments were collected, filled grey circles where measurements of striations on *in situ* shatter cone segments were taken. The traverse along the Parys–Fochville road is also shown (dashed line), along which a number of measurements of angle widths from *in situ* cone segments and samples were taken. Numbers represent the locations mentioned in the text (for locations, see Table 3.1).

Fig. 3.10: (a) and (b) Photograph of a road-cut of rarely exposed shale units of the Witwatersrand Supergroup in the northwestern part of the collar (location 2, see Fig. 3.9, Table 3.1, Appendix No. 6) with abundant striated surfaces that show differences in size, morphology and orientation of apices. The bedding dips with shallow to moderate angles into the photograph.

centre (Gibson 2002; Gibson and Reimold 2005), all indicate the need for some caution in making such an assertion.

Gibson and Reimold (2005) reported that the central parts of the core of the Vredefort Dome experienced shock pressures above 30 – and possibly ≥ 45 – GPa. Average shock pressures appear to have been below 15-20 GPa at distances from the centre of >8 km, and below 10 GPa in the inner collar rocks (>18 -20 km from the centre; see review in Gibson and Reimold 2005). However, as mentioned above, recent results suggest extreme fluctuations in shock pressure on the outcrop and even smaller scales, leading, for example, to local formation of shock melts in both the core (Gibson and Reimold 2005) and collar rocks (Martini 1978, 1991), which makes identification of shock isobars problematic (Gibson and Reimold 2005).

In the course of this study, rare shatter cones were identified as far north as 65 km from the centre of the dome, in Timeball Hill Formation (Transvaal Supergroup) quartzite exposures directly north of the R500 route between Johannesburg and Potchefstroom, northeast of Fochville (Fig. 3.11, location 514 in Fig. 3.9, and Table 3.1). P. Fletcher (Fochville) and W.U. Reimold observed rare but well developed shatter cones immediately west of Bank Station, several kilometres further north from this site. These observations extend the lower shatter cone limit given by Therriault et al. (1997), which was used by these authors to estimate the original diameter of the Vredefort impact structure, by several kilometres. The lithologies hosting these admittedly quite rare shatter cones in the outer collar and even wider environs around the Vredefort Dome do not display any micro-shock deformation features, nor even planar fractures. Lack of calibration of < 5 GPa shock deformation does not allow any better constraints to be placed on the shock barometric limit of these occurrences.

Sagy et al. (2002, 2004) reported shatter cones in basement granitoid gneiss only 15 km from the centre of the dome, but did not provide further information about this specific location. It is suspected that this site could be located in the vicinity of Salvamento Quarry, ca. 5 km northwest of the town of Parys. Indeed, crude, curved, striated fractures were observed in a road-cutting directly west of this quarry (see Fig. 3.9, location 819). Nicolaysen and Reimold (1999) referred to cone-bearing pegmatitic granite in the northern part of the Greenlands greenstone terrane in the far southeastern sector of the core (see Fig. 3.9, location 594), at about 15 km from the centre of the Vredefort Dome and further southeast of this location in metavolcanic greenstones (see also Minnitt et al. 1994; Reimold and Minnitt 1996). W.U. Reimold

(pers. commun. 2004) has observed rare striated fractures throughout the granitoids of the core of the Vredefort Dome. Most involve individual fractures but, very rarely, they involve subparallel sets of quite widely spaced (at several centimetres) striated fractures. Again, such occurrences show a continuum from clearly divergent striae on fractures to subparallel alignment of striations that sometimes closely resembles slickenside striae.



Fig. 3.11: Photograph of a striated surface in Timeball Hill Quartzite (Transvaal Supergroup), about 65 km from the centre of the dome, immediately north of the junction between the R500 and N12 (location 514, see Fig 3.9 and overview map 5.1, and Appendix No. 6). Striations are marked with dashed lines. Bedding dips S-SW. Length of pen ca. 10 cm.

Although commonly well formed in fine-grained rocks (e.g., French 1998; Nicolaysen and Reimold 1999), shatter cones can also be present in the coarser-grained quartzites of the collar. Manton (1965) noted an eccentric distribution of shatter cones in a way that no shatter cones were found in the very mature, clean, and strongly recrystallised Hospital Hill and Orange Grove subgroup quartzites (lowermost in the stratigraphy of the Witwatersrand Supergroup) in the northwestern part of the collar, but with rare exposures of striated surfaces in adjacent quartzites in these subgroups towards the south and southwest of the collar. However, it was found in this investigation that segments of shatter cones are present throughout the collar, including these subgroups, although occurrences in these lithologies are exceedingly

rare (similar to the distribution of shatter cones in the Sudbury Structure, e.g., Dietz 1964). The difficulty in identifying striated surfaces in the latter rocks may be largely due to the locally strongly recrystallized and quite coarse-grained nature of these quartzites.

Some of the best exposures of shatter cones are found in the medium-grained (average matrix grain size ~ 1 mm) quartzites of the Johannesburg and Turffontein subgroups of the upper Witwatersrand Supergroup (Central Rand Group) in the northern and northwestern parts of the collar (locations 519, 279 and 680; see Table 3.1), in the fine-grained (less than 0.1 mm) Booyens Shale Formation (location 2, Fig. 3.9, Table 3.1), and along a road-cut several kilometres north of Schoemansdrift Bridge in the western collar (Jeppestown Subgroup, locations 637-639, showing a shatter cone segment with curved striations; Fig. 3.12). Well-developed cones and closely-spaced fractures also occur in alkali granite of the Schurwedraai complex in the northern part of the collar (see Figs. 3.3a and b, location 402, Fig. 3.9; see also Nicolaysen and Reimold 1999). Here, curved, striated fractures are clearly

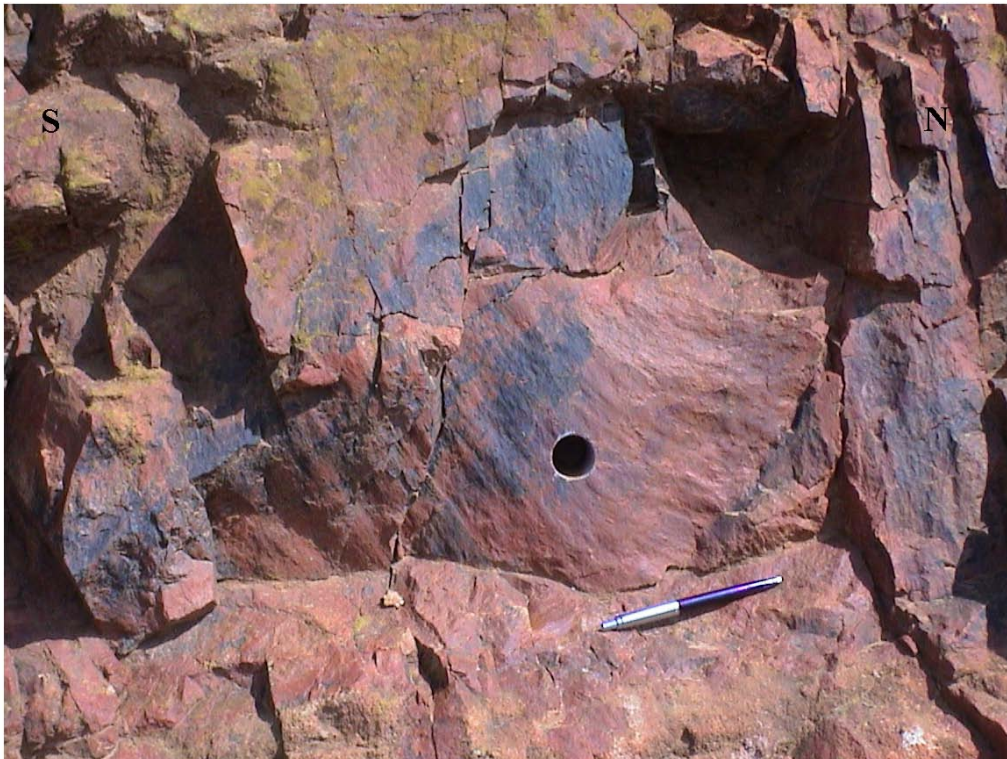


Fig. 3.12: Photograph of a shatter cone in quartzite of the Turffontein Subgroup, ca. 2 km north of the Schoemansdrift Bridge (Location 639, Fig. 3.9, Table 3.1, Appendix No. 6). Note the slightly curved striation pattern at the bottom of the segment. The hole derived from extraction of a sample for a magnetic study. Length of pen ca. 10 cm.

superimposed on pseudotachylitic breccia veins (see also Reimold and Colliston 1994). A meter-sized boulder of alkali granite on farm Kopjeskraal (Gibson and Reimold 2001, Stop 3; location 402, Fig. 3.9) displays closely-spaced striated surfaces of varied orientations; in places, these fracture surfaces have been exposed where this boulder cracked. There, the relationship between striations and closely-spaced fracture surfaces is exceptionally displayed (see below and Figs. 3.3a and b).

3.4.2 Shatter cone morphology

Generally, only parts of shatter cones are exposed in the collar strata, and complete or near-complete cones were not found during this study. The fracture segments are of variable size (ranging from < 5 to > 70 cm, Figs. 3.13a and b) and orientation. The observed shatter cone segments in the collar rocks of the Vredefort Dome commonly display a partially conical form, but range in morphology from paraboloid/hyperboloid forms (Figs. 3.14a and b) to almost planar fracture surfaces (Figs. 3.15a and top segment on b). Figure 3.15a shows an almost perfectly planar striated surface of a sample from the Steinheim Basin in Germany (donated by C. Münchberg, Germany), illustrating that striated but planar surfaces do occur in other impact structures besides Vredefort. Different types of striated surfaces are not restricted to specific sites or areas of the Vredefort collar, but may occur at the same site, within a few decimetres, or even only centimetres, of each other.

Thin sections cut across shatter cone surfaces reveal a very irregular surface form, whereby the surface trace appears to follow the shapes of individual grains. Nicolaysen and Reimold (1999) also noted that fragments of quartz grains had been sheared off and displaced by fractions of a millimetre along some MSJ, indicating that displacement is part of the fracturing process. Similar microscopic to millimetre displacements of quartz grains were also identified during microscopic studies in the course of this project (Figs. 3.16a and b). The fractures penetrate typically the entire sample and cut, in places, through the grains (Fig. 3.16a). Where such fractures branch or interfere, enhanced microfracture density and cataclasis are obvious.

Where a distinct paraboloid geometry is present, apparent apical angles can be measured; they tend to range from 90° to 120° , in agreement with the findings of Manton (1962, 1965) and Albat (1988) from the Vredefort Dome, who advocated a consistent mean angle of about $100^\circ \pm 8^\circ$ at a specific site. However, there is greater variation, although it is only in exceptional instances that narrower ($> 90^\circ$) or wider

Fig. 3.13: The sizes of shatter cone segments range from a few centimetres (a) to several tens of centimetres (b). (a) Photograph of multiple, centimetre-sized shatter cones (so-called horse-tailing) in quartzite of the Turffontein Subgroup at the Schoemansdrift Bridge (location 680, see Appendix No. 6). (b) A several decimetre-sized shatter cone on a boulder in quartzite of the Hospital Hill Subgroup at Donkervliet in the northern part of the collar (near location 11, see Appendix No. 6). Note the curved striation pattern at the bottom of the boulder and compare with Fig. 3.2. Length of pen for scale ca. 10cm.

Fig. 3.14: Photographs of the typical, almost conical shatter cone morphology in the collar of the Vredefort Dome showing typical radial striations branching off a well-defined apex, (a) from the Booyens Shale location (location 2, see Fig. 3.9 and Appendix No. 6), and (b) of a well-developed, decimetre-sized shatter cone segment on a boulder showing diverging striations in quartzite of the Hospital Hill Subgroup in the northern part of the collar (location 404, see Appendix No. 6) ca. 20 km from the centre of the dome. Length of pen for scale ca. 10 cm.

Fig. 3.15: Shatter cone morphology: (a) and (b) give examples of almost parallel striations on a sample from (a) the Steinheim Basin, Germany, and on the top segment of (b) from Vredefort, Booyens Shale location in the northern part of the collar, ca. 30 km away from the centre of the dome (location 2, see Fig. 3.9 and Appendix No. 6).

Fig. 3.16: (a) and (b) Microphotographs of fractures in a shatter cone sample from location 279 (see Fig. 3.9). Section cut perpendicular to striated surface. These pervasive fractures (arrows) are penetrative and usually follow grain boundaries; in places, however, at smaller grains, these fractures may cut through the grain (a). These fractures are filled with dark, oxidic material and show, locally, microscopic to millimetre-scale displacements.

(up to 135°) apex angles have been measured. Naturally, in cases where shatter cone segments are almost planar, with subparallel to parallel striations, it is not possible to determine either an apical angle or even the general orientation of an apex. W.U. Reimold (pers. commun. 2004) recalls one observation in the South Range of Sudbury of an essentially flattened, shield-like occurrence of a three-quarter cone fracture, the apex of which was measured at ca. 160°.

3.4.3 Striation geometries

The geometry of shatter cone striations has been described by many authors as directional and non-parallel (e.g., Albat and Mayer 1989; French 1998). Striations that branch radially off the cone apex (see also Figs. 3.14a and b) do, indeed, form the dominant striation pattern in the samples from the Vredefort Dome. However, the field observations made during this study indicate that the geometry of striations is significantly more diverse (Figs. 3.17a and b). The examples in Figures 3.17a and b illustrate that variable striation geometry does occur on adjacent shatter cone segments and does not depend on the lithology of the host rock. Parallel striations have also been observed on samples from other impact sites, such as from the Steinheim Basin in Germany (example shown in Fig. 3.15a). The sample in Figure 3.17b contains several superimposed cone segments. Whilst the bottom and top segments display striations that are almost parallel to each other, the striations on the surface of the middle segment are clearly divergent.

The striations display variable geometries. Perfectly straight ones occur, but there are also many that are curved towards one side of the surface (see Fig. 3.2). The most common appearance of striations involves divergence from the cone apex. The apex is generally a small area, usually up to half a centimetre wide. In the case of decimetre-sized cones, it may reach several centimetres in width, and it is then typically bounded by a margin formed by several straight segments, resulting in a rather angular shape. Subparallel to almost parallel striations are also common where surfaces are relatively flat (e.g., Figs. 3.15a and b). However, in most cases where shatter cones were found in the Vredefort Dome, the apex area is destroyed, perhaps owing to the extreme energy of a reflected shock wave at this point (as suggested by Baratoux and Melosh 2003; Fig. 3.14a) or due to poor outcrop preservation.

Striation patterns are typically heterogeneous across a given site. Indeed, as the sample in Figure 3.2 clearly demonstrates, a variation from typically divergent to

Fig. 3.17: (a) Photo taken at the Booyens Shale location (location 2, see Fig. 3.9), showing different shatter cone segments directly adjacent to each other; the apices of these two shatter cone surfaces point into two different directions as indicated by arrows. The striation geometry on both adjacent segments ranges from almost parallel (top) to divergent (bottom). Length of pen, for scale, ca. 10 cm. (b) Sample from the northern part of the collar, ca 30 km from the centre of the dome (location 279, see Fig. 3.9, overprinting several shatter cone segments). Their apices point into different directions (marked by arrows). Whilst the top and bottom segments show subparallel striations, the striation pattern on the segment in the centre is divergent.

almost parallel striations may occur at the same site, and even in the same hand specimen. This sample from the Booyens Shale location on farm Rooderand 26 (location 2, Fig. 3.9, Table 3.1) displays characteristic divergent linear striations. However, towards the left of the left set of striations in this image, the striations show a strongly curved, divergent pattern. It appears that the strongly curved parts of striations at the left of this segment lie on a distinct fracture surface, forming a very large, obtuse angle with the fracture surface that carries the straight part of the (NE-trending) striations on the right segment. According to Nicolaysen and Reimold (1999), this curvature would correspond to a combination of striation segments belonging to MSJ of different orientations. The intersection between the two fractures would be located along the solid line in Figure 3.2.

3.4.4 Shatter Cone Orientation

Dietz (1959, 1961) suggested a preferred orientation of the apices of shatter cones upward and outward from the crater centre. Given that the impact typically causes rotation and even overturning of strata at the crater rim, he concluded that rotation of the bedding back to a presumed horizontal pre-impact position would result in a pattern of upward- and inward-pointing cones (see Dietz 1959, 1961; French 1998, and others). In the case of the Vredefort Dome, where the collar rocks and a significant portion of the core rocks have been overturned as a result of central uplift formation (see section 6.2.2), the first attempts at investigating the original orientations of shatter cones by Hargraves (1961) and Manton (1962, 1965) seemed to support the Dietz model.

In contrast, the extensive study by Nicolaysen and Reimold (1999) demonstrated a more diverse orientation of shatter cone apices for a number of specific sites, with areas of detailed study of sometimes not larger than a few square metres extent. Their field observations were confirmed during this study (see Figs. 3.17 and 3.18). For example, Figure 3.18 shows two sets of striated surfaces with different apex orientations. One set is orthogonal to the bedding orientation (which dips into the image) while the other shows apex orientations oblique to the bedding. The orthogonal set would point upwards towards the point of impact when back-rotating the bedding, but the oblique set would be oriented tangential with respect to the centre of the dome.

Striations on shatter cone surfaces from oriented samples analysed in the laboratory as well as from *in situ* cone segments have been measured and plotted onto stereonet. To demonstrate some typical examples of results, orientation measurements from three locations (location 2, location 519 and location 680, see Fig. 3.9) are shown in Figures 3.19a-c.

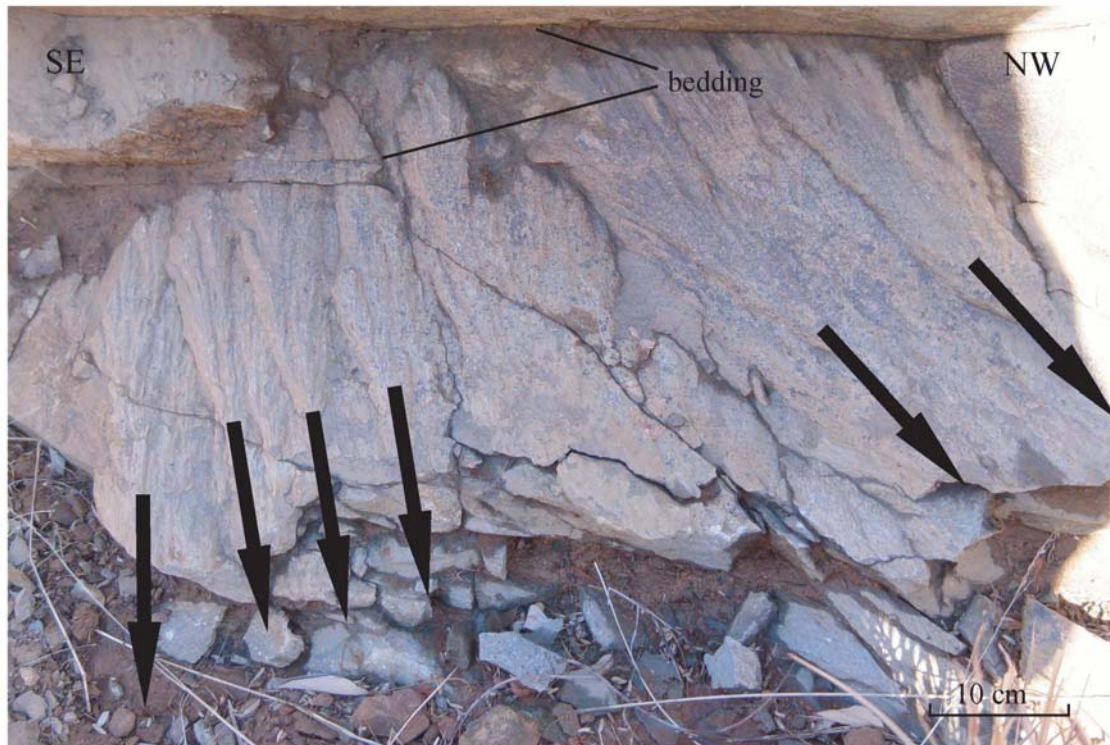


Fig. 3.18: Photograph of shatter cones in the Booyens Shale Formation (location 2, see Fig. 3.9) with orthogonal and oblique orientations of the apices with regard to the bedding. Bedding dips with shallow to moderate angles towards the top of the photograph, i.e., towards the SE, whereas the shatter cone apices show westerly to southwesterly trends (arrows). Photograph courtesy of W.U. Reimold.

Location 2 exposes fine-grained shales of the Booyens Shale Formation of the upper Witwatersrand Supergroup. The outcrop is a continuous, ~150 m long road-cut characterized by widespread and locally intense brittle deformation (see section 2.2.6.1 and Fig. 2.25). Several shear planes at metre-spacing cut through the bedding, but displacements could not be observed. The bedding is strongly overturned with a consistent shallow to moderate southeasterly dip direction and shallow to moderate dip angles (Figs. 3.19a and 2.25).

Shatter cone segments of different size, orientation and form are found. Segments range from a few centimetres up to tens of centimetres in size and show perpendicular and oblique orientations with regard to the bedding (see Figs. 3.17a and

3.18). The forms of the segments range from almost perfectly conical to almost flat surfaces with accordingly divergent to subparallel striations.

Striation measurements from this site, reflecting the overall orientation pattern and the varied form of shatter cone segments, are presented in Fig. 3.19a. Most of the striations are characterized by shallow plunge angles, ranging from 3° to about 20° , with the exception of a set (solid star symbols) that plunges moderately steeply to the

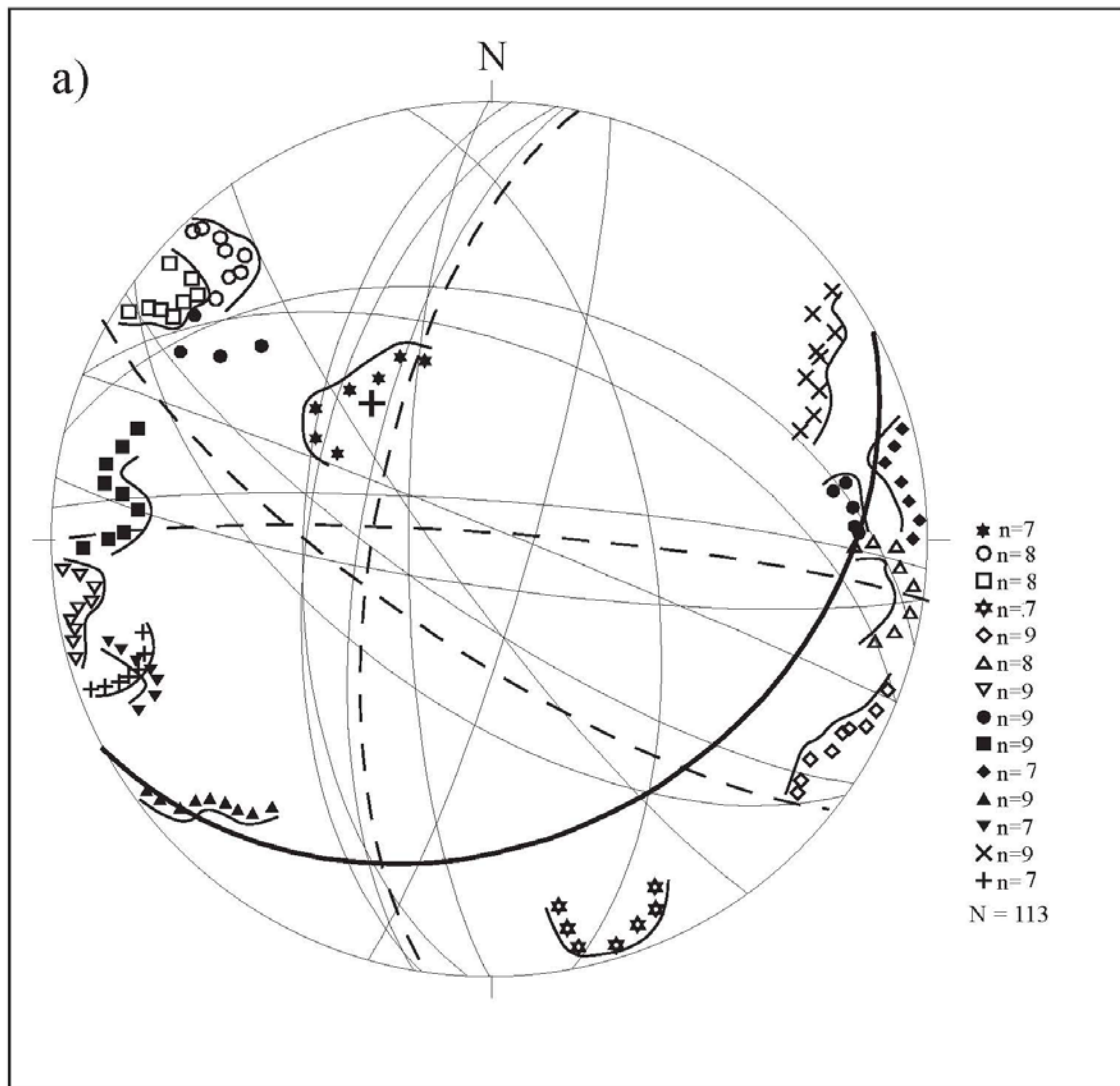


Fig. 3.19: Lower hemisphere equal area projection (Schmidt net) of striations on different cone surfaces at (a) location 2, (b) location 519 (page 151), and (c) location 680 (page 152, see Fig. 3.9). The consistent (average) bedding orientation is marked with a bold cross and a bold great circle. The fracture orientations are given by great circles; orientations of the most prominent large-scale tensile fractures are given by dashed lines. Different symbols represent different shatter cone surfaces and segments, individual data single striation orientations (ridges). Note the generally radial, subhorizontal pattern of striation orientations at location 2. (a) Despite this general attitude it is obviously not possible to construct a well-defined “master-cone” trace without ignoring a large number of data. Striations display a whole variety of shapes of shatter cone surfaces, from typical conical to oscillating or flat, as indicated with thin lines along the trends. For further details, see text.

northwest. The clustering of some striations around the bedding great circle indicates that some of the shatter cone segments actually lie on bedding surfaces. The majority of the striations lie oblique to bedding, with a subset oriented subparallel to the strike of the bedding (Fig. 3.19a).

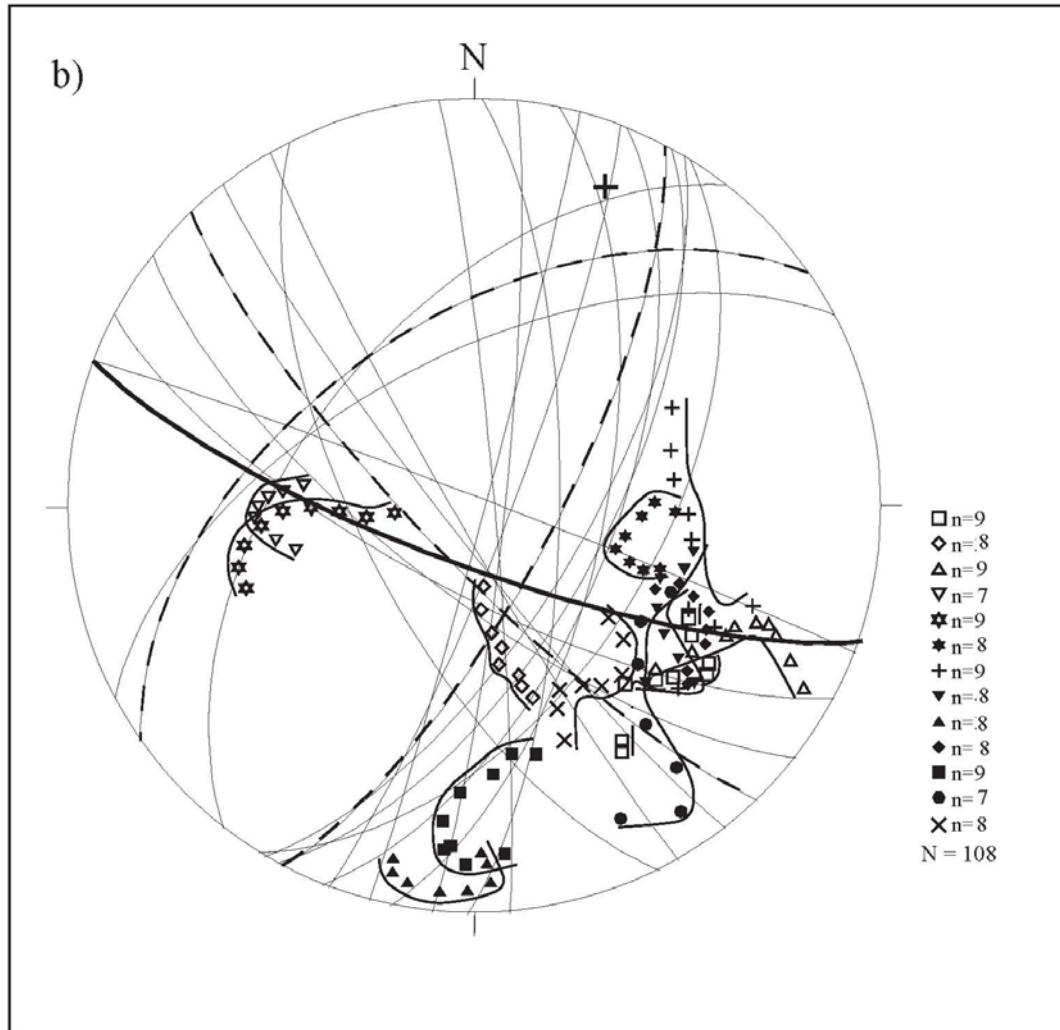


Fig. 3.19 continued from page 150

Striations that do not lie on the bedding surface generally show a close relationship to fractures (Fig. 3.19a) that are closely-spaced (at mm to cm) and mostly do not exceed lengths of a few tens of centimetres. In addition to these small-scale fractures, the other prominent fracture sets in the shales are indicated in Figures 3.19a-c. These fractures crosscut the shatter cones, indicating that they post-date shatter cone formation (see Fig. 3.20; see also chapter 2.7). Most of the larger-scale fractures at location 2, and generally throughout the collar, lie perpendicular, or at high angles, to the bedding (see Fig. 3.19a). These larger-scale fractures can be traced

for up to several metres and are typically straight and pervasive over this distance. They show openings of up to a few millimetres and, thus, are indicative of formation in an extensional environment, and they cross-cut each other (section 2.7). The larger fractures typically occur at tens of centimetres to metre spacings and cross-cut the closely-spaced fractures. The illustrated sets of larger-scale fractures at location 2 (Fig. 3.19a) display a clear cross-cutting relationship with the striated surfaces (Fig. 3.20). Shatter cone-related fractures may not be as prominent as the extensional fractures (see also Nicolaysen and Reimold, 1999) and seem to be restricted to individual layers. In contrast, the extensional fractures cut through multiple sedimentary layers (see Fig. 2.36b).

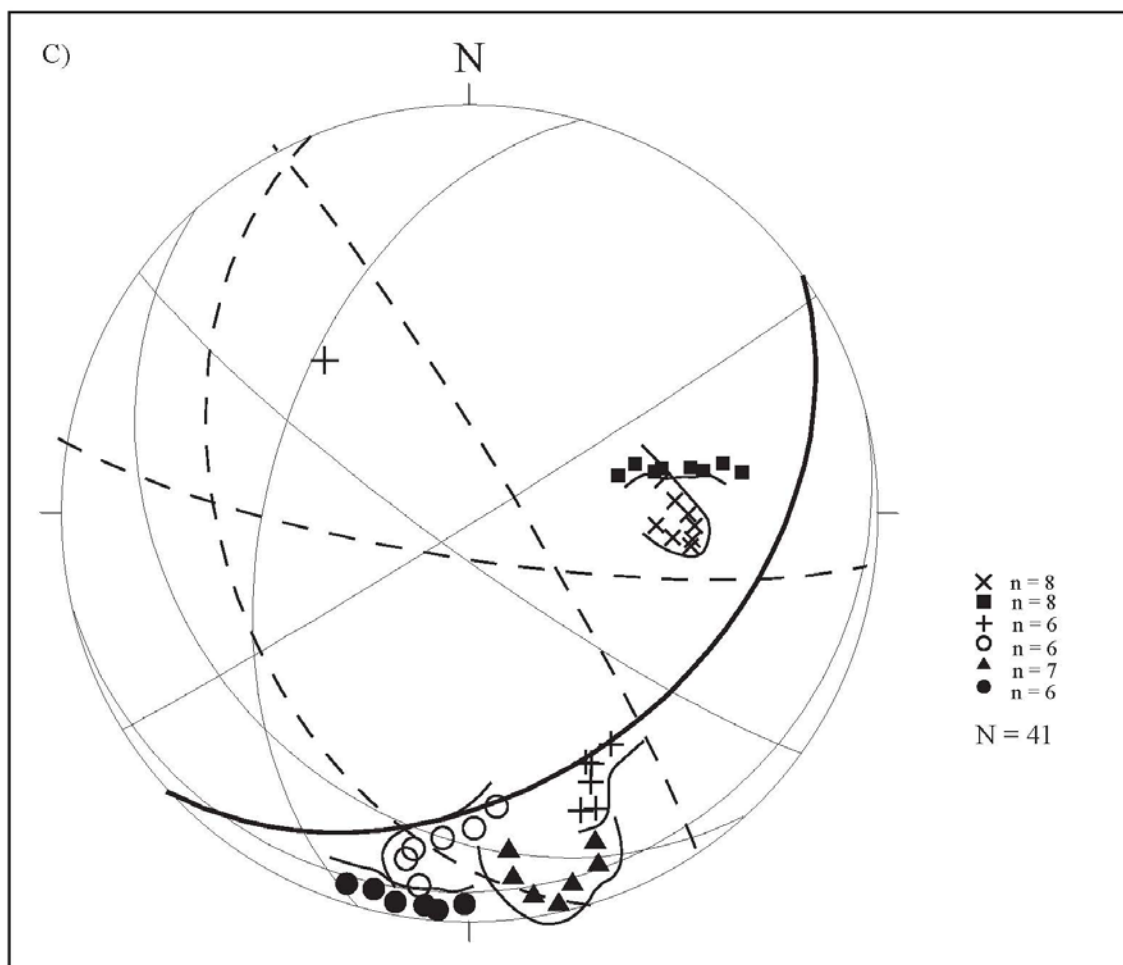


Fig. 3.19 continued from page 150

Location 519 provides very good exposures of shatter cone segments. It is situated in the outer part of the collar, about 35 km from the centre of the impact structure (Fig. 3.9, Table 3.1). Here, fine- to medium-grained quartzite of the

Turffontein Subgroup of the upper Witwatersrand Supergroup is exposed for ~70 m along the Parys-Fochville road. The bedding dips consistently, at moderate angles, to the south-southwest, and is overturned (Fig. 3.19b). Although fault-bounded blocks are quite common in the collar rocks of the Vredefort Dome (also Albat 1988; Albat and Mayer 1989), there is no obvious differential rotation of the bedding along this section, i.e., all measurements of bedding orientations and striated surfaces are from within the same block. The striations at this location (Fig. 3.19b) display a distinctly different pattern to that at location 2 (Fig. 3.19a), in showing steeper overall plunges, but a narrower azimuth range. Moderate to steep plunge angles are most common. Approximately half of the striations lie within the bedding plane but at an oblique angle to the strike of the bedding, i.e., they trend in a WNW-ESE direction, with predominantly moderate plunge angles. However, two clusters of striations display a subhorizontal southerly plunge (filled triangles) and moderate westerly plunge (blank inverted triangles), respectively (Fig. 3.19b).

Some of the striations lie on small-scale fracture sets that are oblique to bedding. However, it seems that, in places, only parts of the segments show a relationship with these joint orientations. The indicated orientations of the post-shatter cone penetrative extensional, large-scale fractures (tens of centimeters to meters; Fig. 3.19b) again show no geometric relationship with the striated surfaces.

Location 680 is situated in the western part of the collar (Fig. 3.9, Table 3.1), ca. 30 km from the centre of the dome. There, the rocks are fine- to medium-grained quartzites of the Turffontein Subgroup. As in the two other cases, a location was chosen where the bedding displays a consistent orientation and is not disturbed or differentially rotated. Overturned bedding dips moderately to the southeast (Fig. 3.19c). A prominent cluster of striations shows a moderate to shallow plunge to the south, whereas a second prominent cluster plunges with a generally moderate angle to the east-northeast. The former cluster of striations is parallel to subparallel to bedding, whereas the latter cluster lies on small-scale fracture sets (Fig. 3.19c). Again, there is no correlation of striations with the large-scale, extensional sets (Fig. 3.19c).

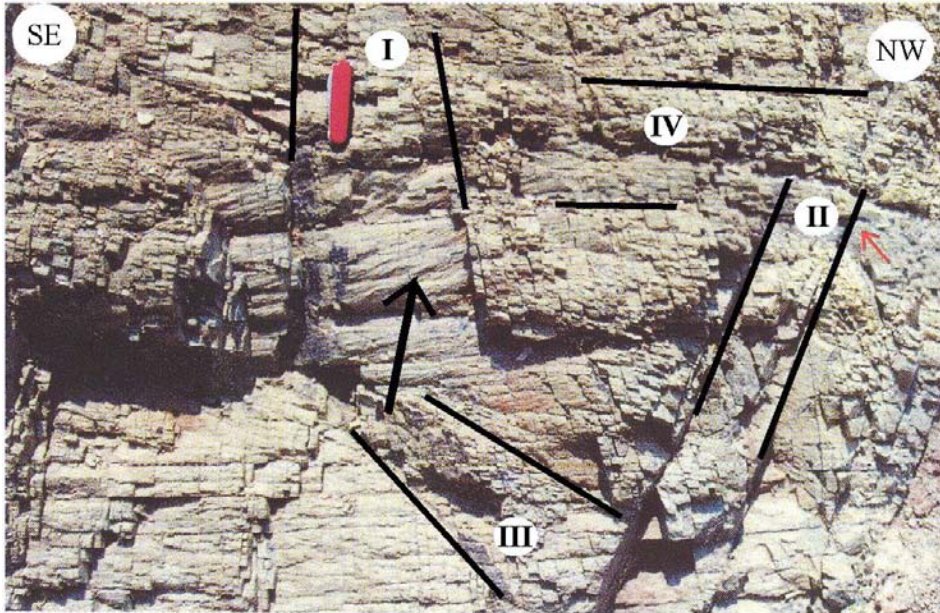


Fig. 3.20: Although shatter cone surfaces show strong relationships with bedding and closely-spaced fracture surfaces, the dominant sets of large-scale tensile fractures (emphasized by lines, see Chapter 2) observed at many places in the collar rocks of the Vredefort Dome crosscut shatter cone segments (e.g. arrow). The vertical (labelled I in Chapter 2) and horizontal (labelled IV in Chapter 2) sets are most intense, with set II trending NNE across the image (right side) and set III only poorly developed (bottom centre). Photograph taken at location 2 (see Fig. 3.9). Length of pocketknife ca. 6 cm (modified after Gibson and Reimold 2001).

3.4.5 Striation angles

Following the suggestion of Sagy et al. (2002, 2004) that the angles between pairs of striations may vary as a function of the distance from the shock source, a large number of angles of striation “ridges”, those V-shaped features delimited by V striation angles, were measured on cones from the Vredefort collar. Striation bundles/ridges are epitomized by the horsetailing patterns known from many impact structures (see Fig. 3.21a, sample from the Steinheim Basin) and that, at Vredefort, are best observed at Schoemansdrift Bridge (location 680, see Fig. 3.9, Table 3.1; Fig. 3.21b). In these cases, striations define apparent “parasitic” cones on a “major cone” or fracture surface, where each parasitic cone apex points towards the apex of the major cone. Sagy et al. (2002) called this pattern a “hierarchical network of secondary branched fractures” (see above and Fig. 3.22).

Widths of so-called striation angles, as defined by Sagy et al. (2002, 2004) were measured on individual samples at different sites throughout the collar and along a traverse along the Fochville-Parys road, extending from 15 to 60 km from the

Fig. 3.21: (a) and (b) Horsetail structures on shatter cone surfaces: from (a) Steinheim Basin, Germany (source of sample: Ries Crater Museum, Nördlingen) and (b), from the Schoemansdrift location, Vredefort Structure (location 680, see Fig. 3.9 and Appendix No. 6). Scales: (a) in cm; (b) pen length ca. 10 cm.

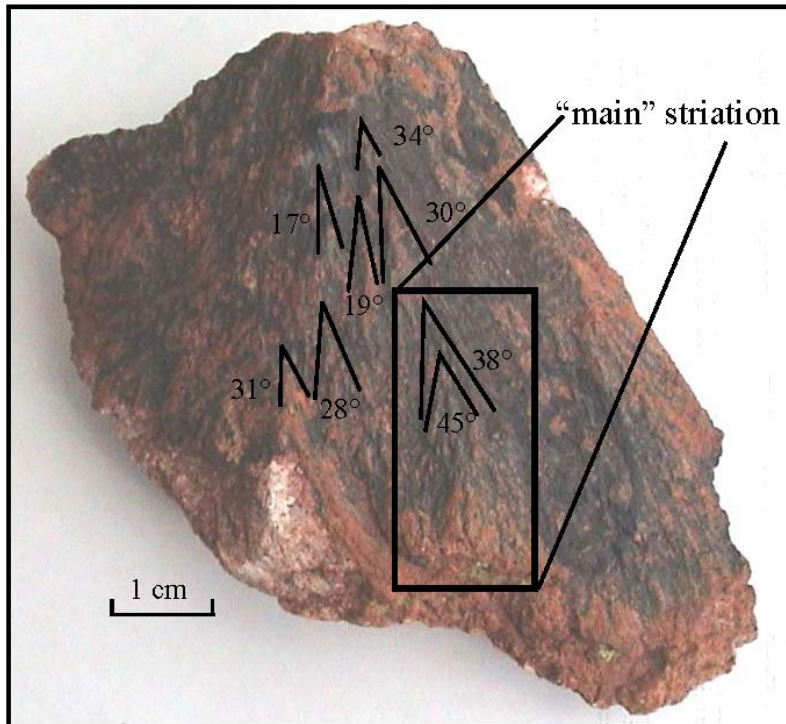


Fig. 3.22: Width of so-called “striation angles” between prominent ridges marking bundles of striations (as marked by frame), defined by Sagy et al. (2002, 2004), on a typical shatter cone segment from the Vredefort Dome (location 500, see Appendix No. 6) in the northwestern part of the collar. The angle width is clearly not consistent on this specimen and ranges from 15° to 45° on the same shatter cone surface (see Appendix No. 5). The frame indicates a “main” striation that consists of several further striations on its flanks showing that striations are not single features on shatter cone segments. The striations are rather formed by bundles of striations and represent a “small-scale” shatter cone themselves where smaller striations branch off the “main” striation.

centre of the dome (Fig. 3.9), in order to test the relationship between angle width and distance from the centre of the impact structure, as proposed by these authors. The striation angle values vary consistently from 20° to 45° on a batch of samples (Fig. 3.22) of the same rock type from a given site and show no consistent variation with radial distance from the centre. Statistical evaluation is exemplified by the data for three samples (Fig. 3.23a-c), one from the greenstone complex in the southeastern core of the Vredefort Dome (location 594, ca. 15 km from the centre, see Fig. 3.9, Table 3.1), one from a Government Reef Subgroup quartzite unit from the northern part of the collar, ca. 27 km from the centre (location 500), and one from the Booyens Formation shale in the northwestern part of the collar (location 2, ca. 30 km from the centre, Fig. 3.9, Table 3.1) (Appendix No. 5). The graph for the greenstone

Fig. 3.23: Statistical evaluation of mean striation angle widths from different locations: (a) A greenstone sample from the Greenlands Complex in the core of the dome (location 594, 15 km from centre, see Fig. 3.9, Table 3.1), (b) a quartzite sample from the Central Rand Group (location 500, 27 km from centre, see Appendix No. 6), and (c) a sample from the shale unit at location 2 (30 km from centre; see Fig. 3.9 and Table 3.1). These histograms clearly show the range of striation angles on these samples and that a mean angle is difficult to determine. Determination of a mean value would require ignoring the actual variety of striation angle widths on each sample.

sample actually shows a bimodal distribution of striation angle values, yielding maxima at $\sim 26^\circ$ and at $\sim 34^\circ$ (Fig. 3.23a), precluding determination of a single mean angle for this sample. If single mean values are calculated, the standard deviation for all samples at these three sites is $\sim 5^\circ$ (for 40 measurements per sample), thus resulting in an overlap of the two means at the greenstone sample. The quartzite sample does indeed have a main peak at $\sim 26^\circ$; however, this statistical value is not truly representative, as lower and higher striation angles are also common (Fig. 3.23b).

The striation angles from the sample of the shale unit show a peak between 20° and 26° , but no values between 36° and 44° (Fig. 3.23c).

The data distribution shows a strong within-site variation of striation angles in at least two of these three cases. The evaluation of mean angles for quartzite units along a traverse through the collar of the Vredefort Dome, with distances ranging from 20 to 60 km (Fig. 3.24), shows the strong irregularity of mean angles over that distance. As the data in Fig. 3.23 clearly show, a calculation of mean angles is difficult and the significance of such values must not be over interpreted. As is evident from Fig. 3.24, different samples from the same location yield significantly different mean striation angles without showing any relationship with regard to the distance of the sample location from the centre of the dome. For comparison, the dependence of striation angles with distance from the centre of the dome, as postulated by Sagy et al. (2002, 2004) for the Vredefort Dome, is illustrated in Figures 3.7 and 3.8. The data of the statistical evaluation of this study clearly demonstrate that the so-called striation angles vary between pairs of striations and between cones at the same site (compare Figs. 3.23a-c and 3.24). Most commonly, the striation angles on a single shatter cone segment vary between 20° and 40° ; but angles varying by as much as from 15° to 45° have been recorded on a single shatter cone from a quartzite unit during this study (Fig. 3.22). Absolute values for the mean striation angle at a given site depend mostly on the subjective selection of measurement sites, because of the significant variation amongst individual striation angles.

3.5 Summary

The observations made during this study demonstrated once more the complexity of the shatter cone phenomenon. Shatter cones were found in all rock types of the collar strata and in all parts of the collar.

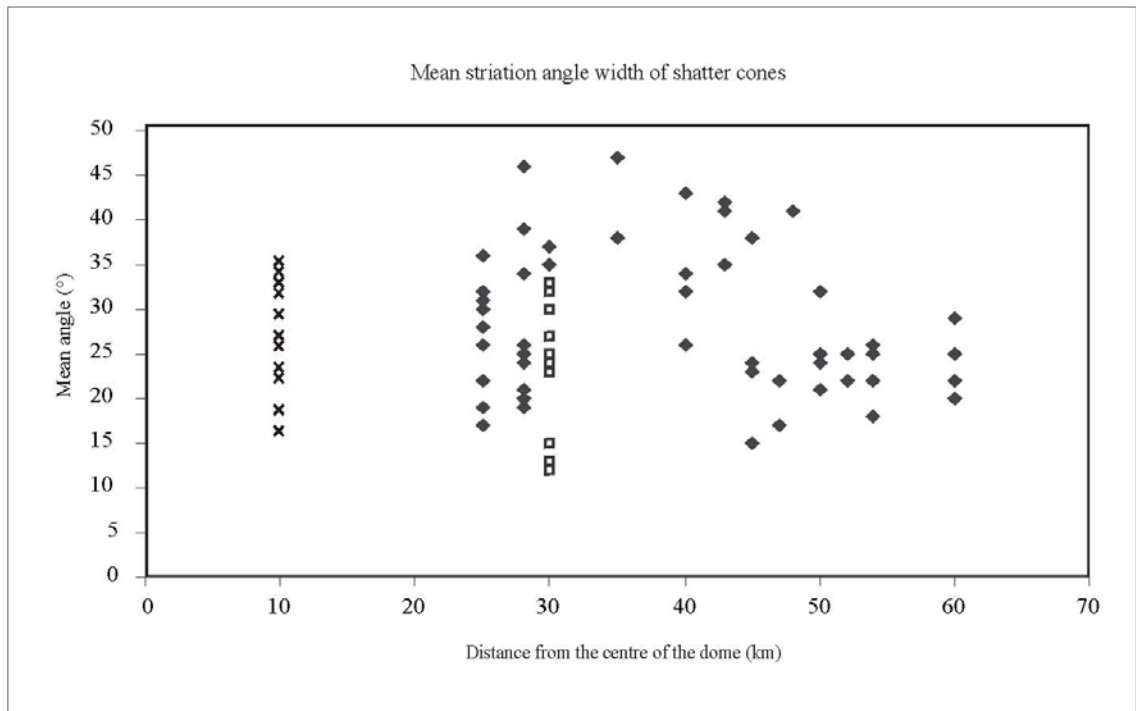


Fig. 3.24: The mean angle width between pairs of striations taken from different sites and different rock types along a traverse along the Parys – Fochville road (up to 60 km from the centre of the dome, see Fig. 3.9). Each symbol represents the mean angle width from one specimen, different symbols correspond to different rock types (crosses – greenstones, filled diamonds – quartzites, open squares – shales).

No complete cone was found, only parts of segments. The shatter cone morphology is not typically conical but ranges from paraboloid/hyperboloid to almost planar surfaces. As a result, the striation pattern on cone surfaces is also variable, ranging from the typically diverging pattern branching off the cone apex to subparallel to parallel striations on almost flat surfaces. The analysis of striations revealed that striations are not single features on shatter cone segments but that they actually represent bundles of striations. These bundles are characterized by smaller-scale striations that branch off the flanks of the main striation, thus giving the appearance of a small-scale shatter cone themselves (see Fig. 3.22).

Contrary to earlier claims, the Vredefort cone fractures do not show uniform apex orientations at any given outcrop. It can be confirmed that the majority of observed striations lie close to bedding, suggesting that bedding-parallel fractures and lithological contacts are prime localities to be exploited by the shock wave. However, striations trending parallel to the strike of the bedding and oblique to it are also frequently observed. Consequently, the model of simple back rotation of the strata to a horizontal pre-impact position does not lead to a uniform centripetal-upward

orientation of the cone apices, as postulated previously (see French 1998 and references therein). Shatter cones also show an orientation pattern at individual locations that cannot be reconciled with the previously postulated “master cone” concept. The striation patterns for different shatter cone segments illustrate the variety of shatter cone forms. Combining the striation orientations, e.g., at location 2, would suggest a crude master-cone with an apex orientation that is roughly vertical and at more than 45° to the bedding surface, and an apical angle that would approach 180°, contrary to the assertions of earlier workers (e.g., Albat 1988). The “master cone” concept is even less favoured by the data from the second prominent location (location 519, see section 3.4.4). If the “master cone” concept is applied to these data, considerable latitude would be required in interpretation, as the data obviously do not lie on a small circle (see Fig. 3.19b).

The evaluation of striation angles on shatter cones demonstrates that the angle does not increase with distance from the crater centre as postulated previously. Instead, individual outcrops present a range of such striation angles, and a more irregular distribution of striation angle values with regard to the distance from the centre of the dome suggests localised controls on this aspect of cone morphology. The results suggests that the formation of striation angles is primarily a function of the shape of the scattered shock wave, and, thus, the nature and shape of the heterogeneity itself, rather than of the intensity and speed of the shock wave travelling through the target rocks (as proposed by Sagy et al. 2002, 2004).

Observations on small-scale structures during this study confirmed the close relationship of shatter cones with curvilinear, closely-spaced fractures (MSJS) as proposed by Nicolaysen and Reimold (1999). Most striated surfaces are found on such fracture surfaces (including bedding surfaces). In contrast, pervasive, centimetre- to metre-scale tensile fractures cross-cut shatter cones and the closely-spaced fractures, and appear to have formed after these structures (see Chapter 2.7).